



Article

Electron-Beam Deposition of Metal and Ceramic-Based Composite Coatings in the Fore-Vacuum Pressure Range

A. V. Tyunkov ¹, A. S. Klimov ¹ , K. P. Savkin ², Y. G. Yushkov ¹ and D. B. Zolotukhin ^{1,*} 

¹ Department of Physics, Tomsk State University of Control Systems and Radioelectronics, Tomsk 634050, Russia

² Institute of High Current Electronics, Tomsk 634050, Russia

* Correspondence: denis.b.zolotukhin@tusur.ru

Abstract: We present the experimental results on the fabrication of metal-ceramic coatings by electron-beam evaporation of alumina ceramic and copper powder composites with different fractions of the components (with Cu powder fraction from 0.1 to 20%) pre-sintered by an electron beam. The mass-to-charge composition of the multi-component plasma, generated in the electron beam transport region, was measured, demonstrating that the fraction of target ions in plasma grows with the electron beam power density. The morphology and electrical conductivity of fabricated coatings were investigated; it was found that the increase in Cu fraction in the deposited coating from 0 to 20% decreases both the volumetric and surface resistance of the coatings in around 8 orders of magnitude, thereby being a convenient tool to control the coating properties.

Keywords: electron-beam evaporation; fore-vacuum pressure range; beam plasma; coating deposition; metal-ceramic coatings



Citation: Tyunkov, A.V.; Klimov, A.S.; Savkin, K.P.; Yushkov, Y.G.; Zolotukhin, D.B. Electron-Beam Deposition of Metal and Ceramic-Based Composite Coatings in the Fore-Vacuum Pressure Range. *Ceramics* **2022**, *5*, 789–797. <https://doi.org/10.3390/ceramics5040057>

Academic Editors: Amirhossein Pakseresht and Kamalan Kirubakaran Amirtharaj Mosas

Received: 26 September 2022

Accepted: 13 October 2022

Published: 17 October 2022

Publisher's Note: MDPI stays neutral with regard to jurisdictional claims in published maps and institutional affiliations.



Copyright: © 2022 by the authors. Licensee MDPI, Basel, Switzerland. This article is an open access article distributed under the terms and conditions of the Creative Commons Attribution (CC BY) license (<https://creativecommons.org/licenses/by/4.0/>).

1. Introduction

Many requirements on industrial products are determined by the properties of the surface layers of the material from which the product is made. The use of expensive and scarce materials in industrial production is often not feasible. In practice, the required properties of a product are achieved by using materials with special coatings that endow such properties [1–3].

Ceramic structures, owing to their high strength properties, are of interest as a reinforcing material in the composites [4,5]. They are refractory, have high specific strength and high mechanical characteristics; they preserve their properties at elevated temperatures. Alumina ceramics is a dielectric, which can be used as an insulating coating in microelectronics [6]. Such coatings can be used for reinforcement, wear-resistance, refractory, optical, biocompatible, and decorative purposes [7–9].

As of today, among the many methods of coating deposition [10–12], beam-plasma methods have a special place. Multifunctional dielectric and metal coatings produced by magnetron or vacuum-arc sputtering and laser ablation in plasma chemical reactors, as well as by electron-beam evaporation, are applied to handle a wide range of practical problems related to surface modification of various materials. In the long list of beam-plasma coating technologies, the electron-beam evaporation technique is characterized by higher rates of deposition and, hence, a higher process performance [13]. The electron-beam evaporation method, when applied to dielectric targets, is hampered by the electron-beam charging of the target surface. To avoid this, it is required to apply, at least at in the initial stages of the technological process, special methods and approaches [14]. It complicates the production equipment and makes the entire process less manageable and efficient.

Fore-vacuum plasma-cathode electron sources [13] can generate electron beams in a previously inaccessible range of elevated fore-vacuum pressures (1–100 Pa). They have all the known advantages of conventional plasma sources of electrons, such as high current

density and reliability and are not demanding in terms of operation in harsh vacuum conditions and in the presence of aggressive gases. The beam plasma generated in the beam transport region at elevated fore-vacuum pressures effectively neutralizes the electron-beam charging of the surface of electrically non-conductive materials [15]. This feature allows one to create plasma that contains evaporation products of a dielectric (ceramics) and deposit its vapor onto the substrate, thus forming a dielectric coating. It is additionally possible, using an electron beam, to create a metal-ceramic coating by evaporating composite targets of compound composition based on ceramic and the addition of practically any metal. The properties of such coatings can be readily controlled by varying the ratio of the components used in the preparation of the target to be evaporated.

In this article, we summarize our studies of the process of obtaining metal-ceramic coatings by electron-beam evaporation of aluminum ceramic and copper composites. The importance of thin films deposited from an evaporated composite target is justified by the fact that the properties of such coatings can be adjusted in a wide range by varying the composition and the fractions of elements in the composite targets.

2. Sample Preparation

The targets for electron beam evaporation were made in our lab from an Al_2O_3 fine dispersive powder with a particle size of $\approx 30\text{--}60\ \mu\text{m}$ and a Cu powder with a particle size of $\approx 30\text{--}50\ \mu\text{m}$. The targets had different weight ratios of metal to ceramics. A total of four targets with different contents of ceramics and metal were used in the experiments. The component composition of the targets is given in Table 1.

Table 1. Component composition of $\text{Al}_2\text{O}_3\text{-Cu}$ targets.

Component	Component Percentage, Mass %			
	Target 1	Target 2	Target 3	Target 4
Al_2O_3	99.9	99	90	80
Cu	0.1	1	10	20

To ensure an even distribution of the material over a target volume, the powder components were mixed for 30 min. Powder was mixed using a conventional ball mill with the addition of ceramic granules. Then, the resulting mixture was poured into a mold and pressed in a pallet at a pressure of 200 MPa. The diameter of the produced target was $10 \pm 0.1\ \text{mm}$ with a height of $3 \pm 0.15\ \text{mm}$. Micrographs of aluminum oxide and copper powders used in the experiment are shown in Figure 1.

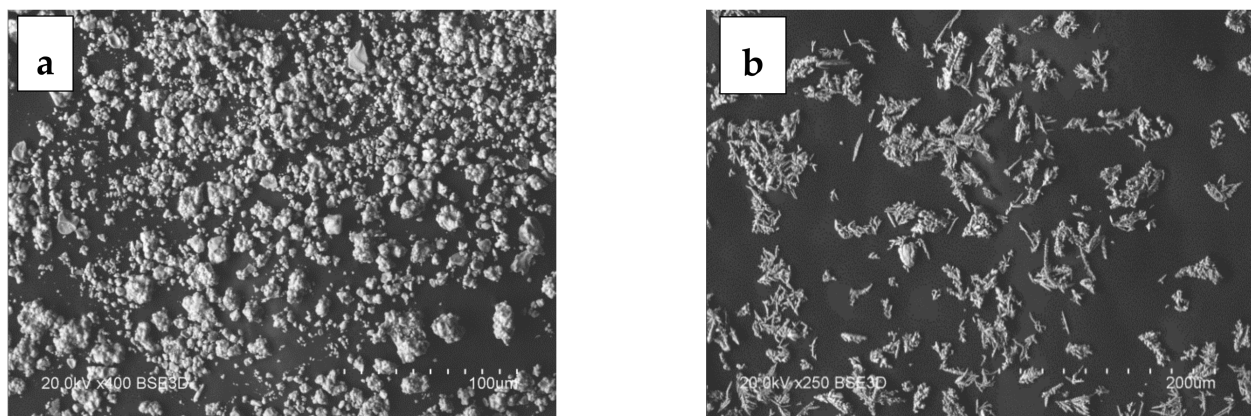


Figure 1. Micrographs of original Al_2O_3 (a) and Cu (b) powders used to fabricate the compacts.

The coatings were deposited on titanium samples (disks, 20 mm in diameter and 3 mm thick), which were located on a stainless holder; it was possible to place up to four samples per cycle. The sample surfaces were prepared using a Sapphire 320 (Germany) grinder and polisher with an automatic RubiN 500 head, with working wheels 200 mm in diameter, the grinder speed 50–600 rev/min and the option to load up to 5 samples per automatic cycle.

The elemental composition of coatings was studied using a Hitachi S3400N SEM, equipped with a BrukerX'Flash 5010 energy-dispersive microanalyzer.

The electrical resistance of the synthesized metal-containing ceramic coatings was studied using an E6-13A teraohmmeter of «Punane-Rat», Estonia. The experimental stand for studying the electrical resistance is discussed in detail in [16].

3. Experimental Setup

Experiments on electron-beam synthesis of coatings were conducted using a fore-vacuum plasma-cathode electron source based on a hollow-cathode glow discharge, operating in a continuous mode [17] (Figure 2). The beam was transported towards the evaporated target at a residual atmosphere of 5 Pa. Under the electron beam action, the target material evaporated and partially ionized, thereby providing the deposition of coating on the sample surface. In one experiment, the coatings were synthesized simultaneously on three samples. The temperatures of the sample surface and of the evaporated target were monitored by a rapid Raytek optical pyrometer; they were 150 and 2100 degrees celsius, respectively. The chamber vacuum was maintained by an ISP-500C spiral fore-vacuum pump. The secondary plasma created during the target material evaporation, consisting of the “products” of the gaseous residual atmosphere and the evaporated target, was analyzed using a modified RGA-300 quadrupole mass-spectrometer, operating as a mass analyzer of the beam plasma ions [18].

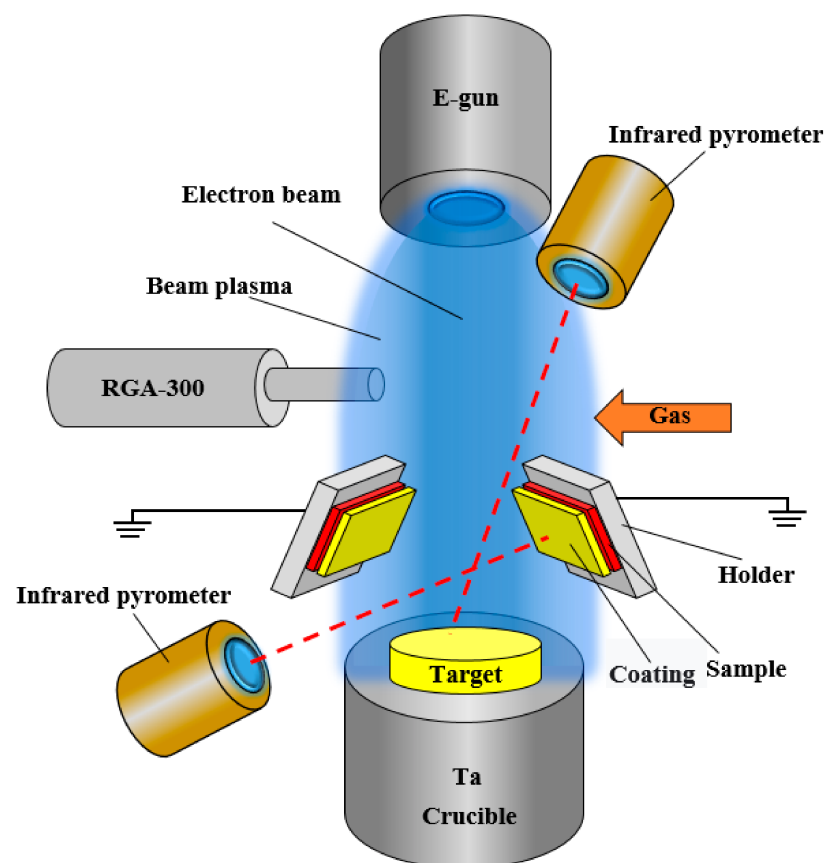


Figure 2. Schematic diagram of the coating deposition experiment.

4. Results

The ion mass-to-charge spectrum of the plasma vapor generated during the electron beam evaporation of target 2 with 1% copper content is shown in Figure 3. This spectrum was recorded during the electron beam evaporation at a power density of 1 kW/cm². As seen, when the evaporation is not intensive, the spectrum includes predominantly ions of the residual atmosphere. The spectrum also registers atomic ions of the ceramic material: lithium, sodium, aluminum, as well as copper. It should be noted that for the indicated copper fraction, the beam power density of about 1 kW/cm² is a threshold value. It is from this level of the power density that the mass analyzer begins to register the copper ions. With a further increase in the electron beam power density, the amplitude of copper ion peaks falls off abruptly against the background of the growing amplitude of aluminum ions.

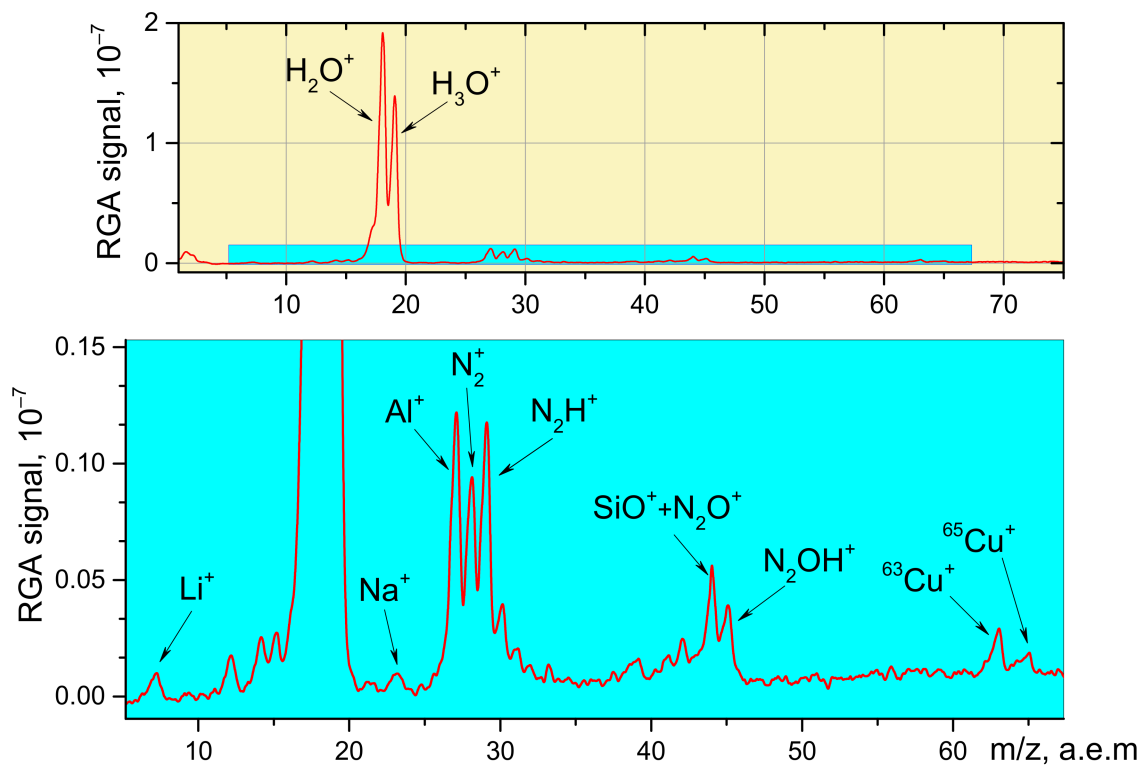


Figure 3. Mass spectrum of the beam plasma ions at a power density of 1 kW/cm².

A similar situation is observed in the plasma generated during the evaporation of target 3 with 10% copper content (Figure 4). At a beam power density of 0.75 kW/cm², the spectrum exhibits exclusively ions of the residual atmosphere. At a beam power density of 1 kW/cm², the spectrum shows the peaks of copper and sodium ions. In contrast to the evaporation of 1% copper target, in this case, the copper peaks are distinctly identified in the spectrum due to the larger fraction of copper atoms. No destruction of the sample surface is observed in this case. As the beam power density increases, the proportion of impurity ions in the spectrum decreases, and the amplitude of ceramic base atoms (aluminum) increases. This fact can be explained as follows. With an increase in the beam power density, the temperature of the target being processed increases. As the temperature increases, fusible (compared to aluminum oxide) impurities (sodium, lithium, copper) melt and, because of differences in the density with the base, move to the surface where they evaporate.

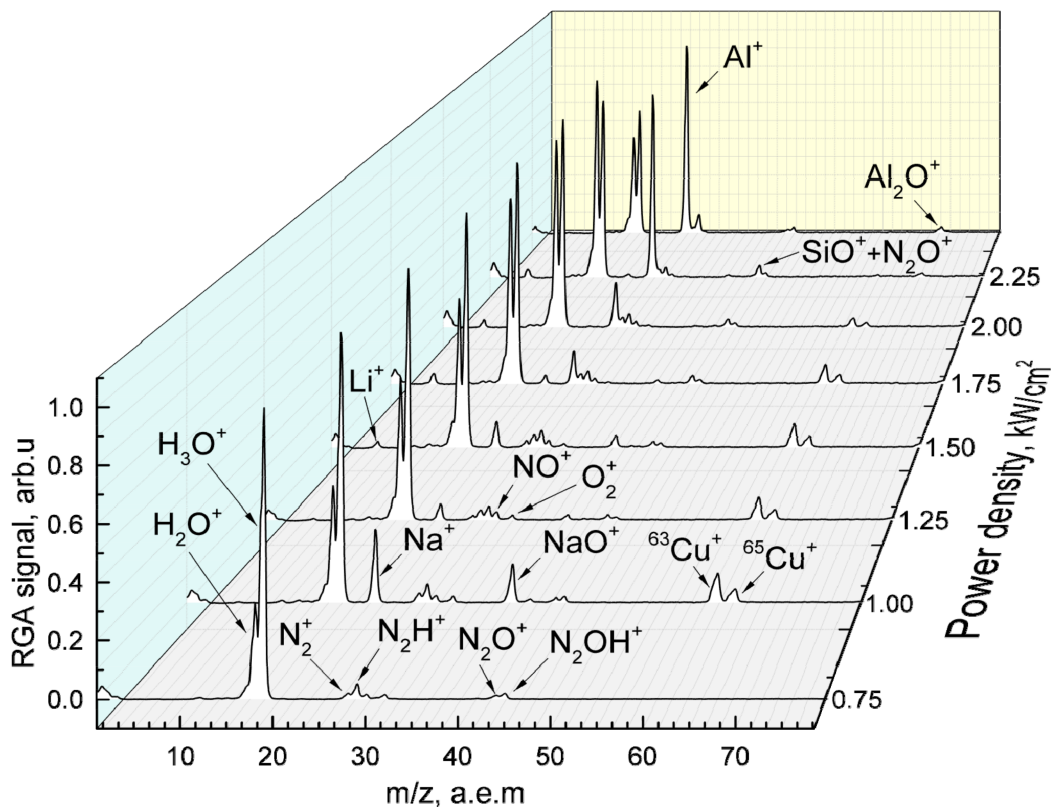


Figure 4. Dependence of the mass-to-charge composition of beam plasma ions on the beam power density.

Since for the case of target 2, the content of such impurities did not exceed 1%, they evaporated within a short time, and the spectra registered only ions of the target material and residual atmosphere. The 10% content of copper in target 3 ensured a longer presence of these ions in the mass-spectra; however, in the end, the ions of the ceramic material remained dominant.

Figure 5 shows typical micrographs of the fabricated coatings depending on the percentage of the components in the target material (see Table 1). As seen, the coating surface is fairly uniform and almost free of defects (Figure 5a–c). Nevertheless, for target 4 with 20% copper (Figure 5d), there are condensed copper droplets on the surface with the size ranging from 500 nm to 2 μm . The coating thickness varies from 1.5 to 2 μm . The deposition rate was greater than 1 μm per minute.

The formation of these droplets on the surface is caused by the explosive boiling of copper in the melting pool of target 4. As a result, along with the vapor or plasma, the micro droplets form, with the velocity comparable to that of copper vapor, and bring about the micro defects in the deposited coating. To reduce this negative effect, one can use high-speed scanning of the target or indirect heating of the target similar to what we used earlier in [19].

Figure 6 shows the elemental composition and its spatial distribution for the obtained coatings. One can conclude from Figure 6 that the components of the evaporated target distributed rather uniformly in the deposited coatings.

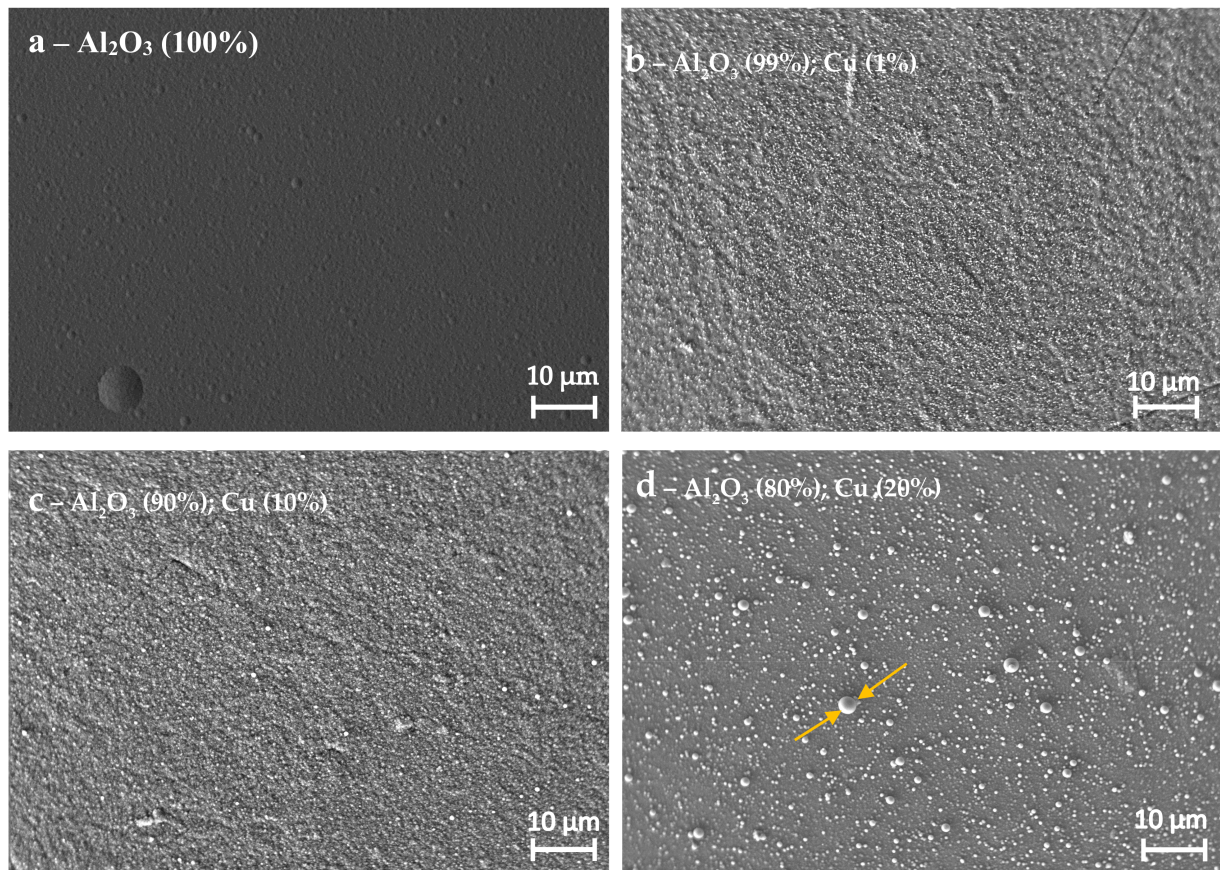


Figure 5. Micrographs of the fabricated coatings.

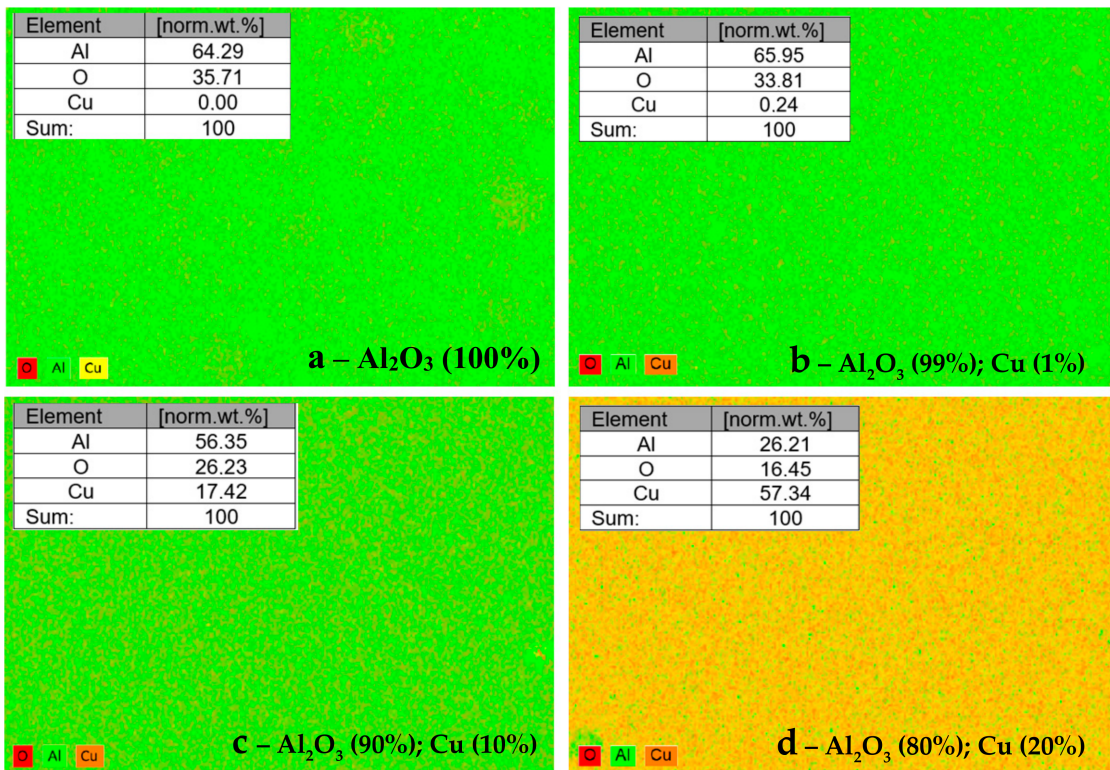


Figure 6. Surface distribution of the coating components.

It should be noted that the copper content in the coatings obtained by the evaporation of targets 3 and 4 (Figure 6c,d) considerably exceeds the copper content in these targets. This is due to a significant difference in melting T_m and boiling T_b points of the components of the target material ($T_m = 1083\text{ }^\circ\text{C}$, $T_b = 2567\text{ }^\circ\text{C}$ for copper; $T_m = 2047\text{ }^\circ\text{C}$, $T_b = 2980\text{ }^\circ\text{C}$ for alumina ceramics). Atoms of relatively fusible copper are quicker to reach the target surface layers during heating, and, hence, they are likely the first to evaporate. Similar to electron beam power density, the density of copper vapor exceeds the density of alumina ceramic vapor, which results in an imbalanced content of elements in the coating and in the target.

The adhesion of metal-ceramic coatings has not been carried out specifically; however, the expression “scratch method”, which consists of applying a linearly-increasing force to the diamond indenter with its simultaneous uniform displacement along the film surface [20], showed that the adhesion of the coatings ranges from 3.2 to 4.1 J/m².

Figure 7 shows the volume and surface resistance of the obtained coatings depending on the fraction of the copper impurity in the target material. For pure ceramic target 1, practically without copper addition, the measured values of the volume and surface resistance of coatings condensed on the surface of titanium samples were at a level of $10^{10}\text{ }\Omega$ and $5 \cdot 10^9\text{ }\Omega/\text{sq}$ (Ohms per square). An increase in the mass fraction of copper in the evaporated target to 1% resulted in a sharp decrease in the volume and surface resistance down to $2 \cdot 10^3\text{ }\Omega$ and $5 \cdot 10^5\text{ }\Omega/\text{sq}$, respectively. A further increase in the proportion of copper in the composite targets to 20% promoted a smoother decrease in electrical resistivity of the deposited coatings down to $10^3\text{ }\Omega/\text{sq}$ for the surface resistance, and to less than $100\text{ }\Omega$ for volume resistance.

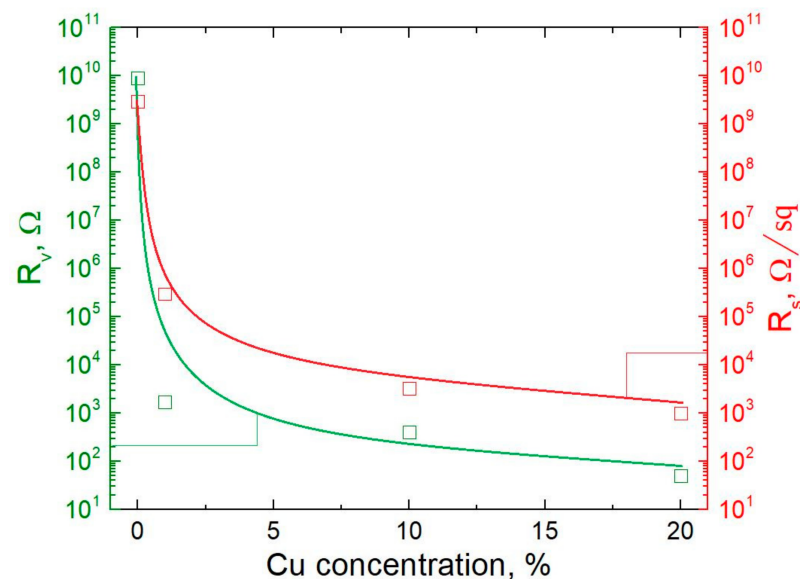


Figure 7. Dependences of the volume and surface resistance on the proportion of copper content in the coating.

We suppose that the main reason for the decrease in the volume resistance is the conductivity matrix, which is created as a result of mutual overlapping of the synthesized copper particles submerged in the bulk of condensed ceramic coating. The surface resistance also decreases with increasing copper proportion in the composite metal-ceramic target as a result of the copper particles residing on the surface of the synthesized coating, and, at the same time, having direct contact with the bulk conductivity matrix consisting of similar particles. Thus, the experimental curves shown in Figure 7 indirectly confirm the correspondence between the stoichiometric composition of the materials of the composite target, subjected to electron-beam evaporation, and the coatings synthesized as a result of condensation of evaporation products.

5. Conclusions

In this article, by example of aluminum oxide ceramics and copper, we present the results of experimental studies that convincingly demonstrate the possibility of fabricating metal-ceramic coatings by electron-beam evaporation of a sintered target, containing powder components of ceramic and metal, in the fore-vacuum pressure range. The mass-to-charge composition of the multicomponent plasma generated in the beam transport region and the morphology and electrical conductivity of obtained coatings were investigated for different ratios of ceramics and copper in the evaporated target. It was experimentally shown that by simply varying the fraction of the metal (copper) within dielectric (alumina) powder, one can predictably control the functional properties (such as volume and surface resistance) of the thin coating deposited on a substrate as a result of electron beam evaporation of the mixed-powder target. These results justify the further search of possibilities to control other properties (such as porosity, hardness, Young modulus, corrosion resistance, etc.) by the choice of proper materials and their fractions in the composite target. The results of the studies carried out expand the field of the possible applications of electron-beam synthesis of functional coatings using fore-vacuum plasma-cathode electron sources.

Author Contributions: Conceptualization, A.V.T. and Y.G.Y.; methodology, A.S.K. and K.P.S.; validation, A.V.T., K.P.S. and Y.G.Y.; investigation, A.V.T.; data curation, K.P.S.; writing—original draft preparation, A.V.T.; writing—review and editing, D.B.Z.; visualization, A.V.T.; supervision, Y.G.Y.; project administration, Y.G.Y.; funding acquisition, Y.G.Y. All authors have read and agreed to the published version of the manuscript.

Funding: The research of plasma parameters were supported by the program of the Ministry of Science and High Education of Russian Federation for youth laboratories, Project No. FEWM-2021–0013. The coating fabrication and studies were supported by the Russian Science Foundation (Grant No. 21-79-1003 5), <https://rscf.ru/project/21-79-10035/>.

Institutional Review Board Statement: Not applicable.

Informed Consent Statement: Not applicable.

Data Availability Statement: Data are available upon reasonable request.

Conflicts of Interest: The authors declare no conflict of interest.

References

1. Tejero-Martin, D.; Bennett, C.; Hussain, T. A review on environmental barrier coatings: History, current state of the art and future developments. *J. Eur. Ceram. Soc.* **2021**, *41*, 1747–1768. [[CrossRef](#)]
2. Lee, K.N.; Miller, R.A.; Jacobson, N.S.; Opila, E.J. Environmental durability of mullite coating/SiC and mullite-YSZ coating/SiC systems. *Ceram. Eng. Sci. Proc.* **1995**, *16*, 1037–1044. [[CrossRef](#)]
3. Lee, K.N. Current status of environmental barrier coatings for Si-Based ceramics. *Surf. Coat. Technol.* **2000**, *133*, 1–7. [[CrossRef](#)]
4. Lee, K.N.; Fox, D.S.; Robinson, R.C.; Bansal, N.P. Environmental barrier coatings for silicon-based ceramics. In *High Temp. Ceram. Matrix Compos*; Wiley-VCH Verlag GmbH & Co. KGaA: Weinheim, Germany, 2006; pp. 224–229. [[CrossRef](#)]
5. Krause, A.R.; Garces, H.F.; Senturk, B.S.; Padture, N.P. 2ZrO₂·Y₂O₃ thermal barrier coatings resistant to degradation by molten CMAS: Part II, interactions with sand and fly ash. *J. Am. Ceram. Soc.* **2014**, *97*, 3950–3957. [[CrossRef](#)]
6. Yushkov, Y.G.; Oks, E.M.; Tyunkov, A.V.; Yushenko, A.Y.; Zolotukhin, D.B. Electron-Beam Deposition of Aluminum Nitride and Oxide Ceramic Coatings for Microelectronic Devices. *Coatings* **2021**, *11*, 645. [[CrossRef](#)]
7. Padture, N.P. Advanced structural ceramics in aerospace propulsion. *Nat. Mater.* **2016**, *15*, 804–809. [[CrossRef](#)] [[PubMed](#)]
8. Sundaram, K.B.; Alizadeh, J. Deposition and optical studies of silicon carbide nitride thin films. *Thin Solid Films* **2000**, *370*, 151–154. [[CrossRef](#)]
9. Hou, N.Y.; Perinpanayagam, H.; Mozumder, M.S.; Zhu, J. Novel Development of Biocompatible Coatings for Bone Implants. *Coatings* **2015**, *5*, 737–757. [[CrossRef](#)]
10. Yushkov, Y.G.; Oks, E.M.; Tyunkov, A.V.; Zolotukhin, D.B. Electron-Beam Synthesis of Dielectric Coatings Using Forevacuum Plasma Electron Sources (Review). *Coatings* **2022**, *12*, 82. [[CrossRef](#)]
11. Anders, A. Physics of arcing, and implications to sputter deposition. *Thin Solid Films* **2006**, *502*, 22–28. [[CrossRef](#)]
12. Kelly, P.J.; Arnell, R.D. Magnetron sputtering: A review of recent developments and applications. *Vacuum* **2000**, *56*, 159–172. [[CrossRef](#)]
13. Yushkov, Y.G.; Oks, E.M.; Tyunkov, A.V.; Zolotukhin, D.B. Alumina Coating Deposition by Electron-Beam Evaporation of Ceramic Using a Forevacuum Plasma-Cathode Electron Source. *Ceram. Int.* **2019**, *45*, 9782–9787. [[CrossRef](#)]

14. Burdovitsin, V.A.; Medovnik, A.V.; Oks, E.M.; Skrobov, E.V.; Yushkov, Y.G. Potential of a Dielectric Target during Its Irradiation by a Pulsed Electron Beam in the Forevacuum Pressure Range. *Tech. Phys.* **2012**, *57*, 1424–1429. [[CrossRef](#)]
15. Yushkov, Y.G.; Oks, E.M.; Tyunkov, A.V. Deposition of Boron-Containing Coatings by Electron-Beam Evaporation of Boron-Containing Targets. *Ceram. Int.* **2020**, *46*, 4519–4525. [[CrossRef](#)]
16. Savkin, K.P.; Bugaev, A.S.; Nikolaev, A.G.; Oks, E.M.; Kurzina, I.A.; Shandrikov, M.V.; Yushkov, G.Y.; Brown, I.G. Decrease of ceramic surface resistance by implantation using a vacuum arc metal ion source. In Proceedings of the 2012 25th International Symposium on Discharges and Electrical Insulation in Vacuum (ISDEIV), Tomsk, Russia, 2–7 September 2012; pp. 554–557. [[CrossRef](#)]
17. Zolotukhin, D.B.; Oks, E.M.; Tyunkov, A.V.; Yushkov, Y.G. Deposition of Dielectric Films on Silicon Using a Fore-Vacuum Plasma Electron Source. *Rev. Sci. Instrum.* **2016**, *87*, 063302. [[CrossRef](#)] [[PubMed](#)]
18. Tyunkov, A.V.; Oks, E.M.; Yushkov, Y.G.; Zolotukhin, D.B. Ion Composition of the Beam Plasma Generated by Electron-Beam Evaporation of Metals and Ceramic in the Forevacuum Range of Pressure. *Catalysts* **2022**, *12*, 574. [[CrossRef](#)]
19. Tyunkov, A.V.; Yushkov, Y.G.; Zolotukhin, D.B. Generation of Metal Ions in the Beam Plasma Produced by a Forevacuum-Pressure Electron Beam Source. *Phys. Plasmas* **2014**, *21*, 123115. [[CrossRef](#)]
20. Yushkov, Y.G.; Oks, E.M.; Tyunkov, A.V.; Zolotukhin, D.B. Dielectric Coating Deposition Regimes during Electron-Beam Evaporation of Ceramics in the Fore-Vacuum Pressure Range. *Coatings* **2022**, *12*, 130. [[CrossRef](#)]